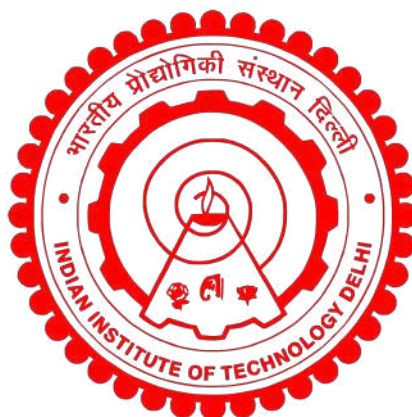


**COMPUTATIONAL INVESTIGATION OF
MOLECULAR CROWDING EFFECTS ON
MACROMOLECULAR
CONFORMATIONAL EQUILIBRIA AND
SELF-ASSEMBLY**

SATYENDRA RAJPUT



Department of Materials Science and Engineering
INDIAN INSTITUTE OF TECHNOLOGY DELHI
JUNE 2025

© Indian Institute of Technology Delhi (IITD), New Delhi, 2025

**COMPUTATIONAL INVESTIGATION OF
MOLECULAR CROWDING EFFECTS ON
MACROMOLECULAR
CONFORMATIONAL EQUILIBRIA AND
SELF-ASSEMBLY**

by

SATYENDRA RAJPUT

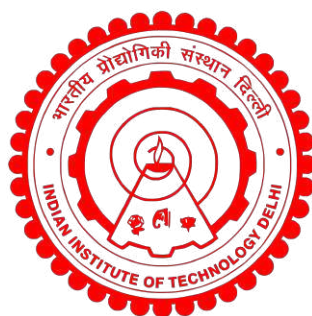
**Department of Materials Science and
Engineering**

Submitted

in fulfillment of the requirements of the degree of

Doctor of Philosophy

to the



**INDIAN INSTITUTE OF TECHNOLOGY DELHI
JUNE 2025**

Certificate

This is to certify that the Thesis titled "**COMPUTATIONAL INVESTIGATION OF MOLECULAR CROWDING EFFECTS ON MACROMOLECULAR CONFORMATIONAL EQUILIBRIA AND SELF-ASSEMBLY**" is being submitted by **Mr. Satyendra Rajput** to the Department of Materials Science & Engineering, Indian Institute of Technology Delhi, for the award of the degree of **Doctor of Philosophy**. This Thesis is a record of bona-fide research work carried out by him under my guidance and supervision. In my opinion, his Thesis has reached the standards that fulfill the requirements of the regulations relating to the degree.

The results contained in this Thesis have not been submitted to any other University or Institute for the award of any degree or diploma.

Date:

New Delhi

Dr. Divya Nayar

Assistant Professor
Department of Materials Science & Engineering
Indian Institute of Technology Delhi
New Delhi-110 016

*Everything comes to us that belongs to us,
if we create the capacity to receive it.*

Rabindranath Tagore

*Dedicated to My family,
friends, and all my well-wishers*

ACKNOWLEDGMENTS

As I am near to completion of nearly five years or so at the Indian Institute of Technology Delhi (IIT Delhi), New Delhi, as a research scholar in the Department of Materials Science & Engineering (DMSE), I find myself reflecting on a journey filled with wisdom, learning, discovery, and immense joy. Working here, in an environment brimming with vibrant energy and limitless scientific curiosity, has been both a privilege and an adventure. The countless discussions, challenges, and moments of insight have made this experience not just an academic pursuit but a deeply fulfilled journey. This Thesis would not have been possible without the unwavering support, encouragement, and unconditional love of those in my nearest solvation shells—mentors, colleagues, friends, and family who have stood by me through ups and downs. I am profoundly grateful to each of them and take this moment to acknowledge their invaluable presence in shaping this endeavor.

First and foremost, I extend my deepest gratitude to my supervisor, Prof. Divya Nayar, for her unwavering support, insightful guidance, and endless patience. A visionary mentor and exceptional educator, she has been the cornerstone of my research journey, providing wisdom, knowledge, encouragement, and a steady source of inspiration. She is a great advisor with remarkable vision and a calm personality as deep and steady as the ocean. I am profoundly grateful for her unconditional support, invaluable guidance, and selfless efforts, which have made this Thesis possible. To me, she represents the pinnacle of excellence, dedication, perseverance, and optimism. Her remarkable qualities have motivated me to evolve, not just as a researcher, but also as a more thoughtful and compassionate individual and as a good human being. Her constant encouragement has opened my mind to new perspectives in science, learned to make wiser decisions, and empowered me to pursue my dreams with crystal clear clarity. I feel incredibly blessed and honored to be the her very first student. I am fortunate enough to work in such a warm, intellectual environment, surrounded by brilliant and inquisitive minds. I will always take immense pride in being your student and a member of your research group. Your encouragement gave me the freedom to explore, the confidence to grow, while your readiness to offer guidance and support was a constant reassurance. Words cannot fully express my gratitude for all these years.

My heartfelt thanks to Prof. Ram Ramaswamy for inspiring me as a student from my M.Sc. days at JNU, New Delhi. His guidance not only shaped

my academic path but also sparked a passion for science that continues to drive me today. I would like to express my deepest gratitude to my research committee members Prof. Pramit K. Chowdhury (Department of Chemistry), Prof. Leena Nebhani (Department of Materials Science & Engineering), and Prof. Nirat Ray (Department of Materials Science & Engineering) for their insightful feedback and invaluable suggestions throughout my comprehensive and synopsis presentations. Their intriguing questions pushed me to expand my thinking out of the box, which greatly enriched my work. A special thanks to Prof. Pramit K. Chowdhury (Dept. of Chemistry) for his profound discussions, brilliant suggestions, and thought-provoking insights into my research. I also want to extend my thanks to the faculty members of the Department of Materials Science & Engineering, Computer Service Center, and Department of Chemistry, whose courses and workshops were essential in shaping my understanding and laying the foundational work for my research. My sincere thanks also go to the DRC chairperson, Prof. Leena Nebhani, the entire faculty members, and non-academic staff of the Department of Materials Science & Engineering for their continuous support and guidance throughout my Ph.D. journey.

I sincerely appreciate to Computer Service Center at IIT Delhi for providing me the high-performance computing facilities and resources, without which the work of this Thesis would not have been possible. I am also grateful to the IIT Delhi Library for granting unlimited access to journals, which have formed the backbone of this Thesis. I also extend my thanks to the academic and non-academic staff members of IIT Delhi for their support in handling the administrative work involved during my Ph.D. I am also thankful to IIT Delhi for providing the junior and senior research fellowship. Additionally, I express my gratitude to the Anusandhan National Research Foundation (ANRF) for funding my participation in an international conference.

I am also grateful to our collaborators from Germany, Prof. Klaus Huber and Prof. Simon Ebbinghaus, along with their research groups, for providing support through experimental validation and for the fruitful discussions that have enriched this research.

The contributions of my fellow lab mates to my Ph.D. journey are invaluable and deeply cherished. I would like to begin by expressing my heartfelt gratitude to Mr. Siba Sankar Panigrahy, who has supported me from the very beginning of my Ph.D. to its completion. His mentorship has been instrumental in the successful completion of this Thesis. Siba not only trained me to work confidently in the lab but also generously shared his extensive

knowledge on various subjects. His guidance, filled with care and wisdom, made him as a second mentor to me. I am equally grateful to Ms. Gunjana Yadav, who played a crucial role in my Ph.D. journey. She was a constant source of motivation, uplifting my spirits when challenges felt overwhelming and providing invaluable assistance throughout the process.

A special note of thanks to Shivnandi, with whom I have shared a greater number of lunches; Abhay Chauhan – for his great humor, engaging scientific and non-scientific discussions, and keeping me updated on every cricket match; Archana Karki – for her sincerity, hard work, and sharing inspirational stories from her hometown while contributing to a friendly and vibrant lab environment. Working alongside Priya Benny C. on the same project was a pleasure; her reliability as both a friend and colleague was truly invaluable. I am also deeply grateful to Alen James, Dhiliban L., Peteti Yogananda, Shubham Suthar, and Vishal for their consistent support in navigating the complexities of my research, whether through insightful discussions, technical assistance, or simply being there in a challenging time. I extend my appreciation to all my fellow lab mates for the insightful discussions that enhanced my understanding and contributed to the progress of my work. I am also grateful to our former postdoctoral fellow, Andri Sharma, and to Shweta for helping me explore other scientific areas and for their support during scientific challenges. Additionally, I thank the summer students and M.Sc. students for bringing enthusiasm and excitement to research, which was both inspiring and motivating.

I also deeply appreciate my previous supervisors from my masters studies, Prof. Amar Nath Gupta (IIT Kharagpur) and Prof. Poonam Mehta (SPS, JNU), whose encouragement and guidance laid a strong foundation for this journey.

I am also grateful to Prof. Faraz Ahmed Inam (AMU) for his unwavering support, which has remained constant from my graduation days to the present. I would not be who I am today without the blessings of my school-teachers Mr. Rajveer Singh, Mr. Shailendra Yadav, and Mr. Shushil Yadav. They provided essential guidance and support, nurturing my growth – much like a seed growing into a strong tree. This journey would not have been possible without these unsung heroes of my life.

My deepest gratitude goes to Room No. D–9 of Jeet Ram House, where I spent nearly four and a half years until the completion of my Thesis. This place holds a special significance for me, enriched with love, patience, late-night study, and the warmth of friendships that made this journey unforget-

table. I would like to extend my heartfelt thanks to my dear friends who have stood by me through the ups and downs of both my professional and personal journey: Dr. Arvind Patel, Dr. Kamal Kishor, Dr. Shailendra Pal, Dr. Satish Kumar, Dr. Mohd. Noor, Dr. Tawseef Wani, Dr. Vivek, Brijesh, Satvik, Mohit, Lav Kumar, Saurvendra, Devesh, Arvind, Dr. Manisha, Mahendra, and Sachin.

To my friends at IIT – Kartikey Singh, Vaibhav, Arun, Srest, Harshita, Shweta, Soumya, Saurabh, Tajamul, and Suraj—your friendship has been a pillar of immense support. I would also like to thank Chhotarai Soren, who has always been ready for a cycle trip. Additionally, I am grateful to Dr. A. Sudha, who is always just an email away and ready to assist in times of need.

I would also like to mention my friends from JNU—Avdhesh, Dr. Vandu, Pravi, Dr. Rahul, Dr. Sudipto, Dr. Surojit, Abhinash, Ankita, Saket, Dr. Amit, Ajay, Sabila, and Ankit—thank you for your unwavering encouragement, even after all this time.

I would like to express my heartfelt gratitude to everyone who has contributed to this Thesis through their constant encouragement and support.

Above all, I thank my family for being my pillar of strength throughout my Ph.D. journey. I am especially grateful to my grandparents, and parents, who instilled in me the values of education and hard work, and whose unwavering love and encouragement have been my greatest source of motivation. I also deeply appreciate my siblings (Anita, and Chandra Shekhar) for their sacrifices, support, blessings, and guidance, which have played a crucial role in making this Thesis possible. A special thanks to my sister-in-law (Sarita), and my nephew and niece (Shreyansh and Shreyanshi), for their unwavering love and support, which brought me joy and strength throughout this journey.

And finally, I should thank myself for making this Thesis!

Satyendra Rajput

संक्षेपः

न्यूक्लियक अम्लम्, प्रोटीन्, बहुपरिणिकाः, लघुचयापचयद्रव्याणि इत्यादीनां कठिनतया पैक्ड जै-वअणुकानां उच्चसान्द्रतायाः (३०० -- ४०० ग्राम/लीटरस्य) कारणेन अन्तःकोशिकीयवा-तावरणं “जनसङ्ख्यायुक्तं” इति मन्यते। प्रोटीन-तन्त्र-सदृशानां प्रक्रियाणां ऊष्मागतिकी-गतिविज्ञानयोः उपरि भीड-परिवेशस्य प्रभावः अधिकाधिकं ज्ञायते। सुप्रतिष्ठिताः भीडस्य प्रभावेषु जैवअणुनां संकुचनं भवति यत् तेषां आकारस्य कारणेन संकुचकानां एन्ट्रोपिक् बहिष्कृत आयत-नप्रभावैः उत्पद्यते। अद्यतन अन्वेषणैः तु सूचितम् अस्ति एतादृशेषु जटिलतन्त्रेषु मृदु ऊर्जायुक्ता-नां अन्तरक्रियाणां महत्त्वम्। अतः एतेषां प्रभावानां व्यापकसूक्ष्मदृष्टिकोणबोधः अद्यापि दुर्गमः एव अस्ति। अस्मिन् प्रबन्धे, अस्माभिः आणविकगतिविज्ञानस्य अनुकरणस्य उपयोगेन स्थूलअ-णुकानां स्वसङ्घटनस्य पतनस्य च उपरि आणविकसङ्कुलस्य प्रभावस्य अन्वेषणं कृतम् अस्ति। एतस्याः घटनायाः अन्वेषणार्थं सरलीकृतविलेयप्रतिमानानाम् विचारः कृतः, यथा कार्बनिक-कैटियन-छन्न-आइसोसायनिन्-क्लोराइड (PIC) रञ्जकः, यः आन्तरिकरूपेण अव्यवस्थितप्रो-टीनानां सदृशानि रेशेन-सदृशानि संरचनानि निर्माति, यत् प्रोटीन-सङ्ग्रहणस्य अन्वेषणं प्र-दाति। आणविक-क्राउडररूपेण एथिलीन-ग्लाइकोलस्य मृदु-आकर्षक-अविशिष्ट-अन्तर्क्रियाः रञ्जक-ओलिगोमेराइजेशनं प्रतिकूलं कुर्वन्ति इति ज्ञातम्। रञ्जक-क्राउडर-आकर्षक-परस्परक्रियाभिः रञ्जक-ओलिगोमेर-जलीकरण-घनत्वं न्यूनीकृतम्, येन ऊर्जावानः दण्डः उत्पन्नः यः भीड-विलयनेषु रञ्जक-अतिगुणीकरणस्य प्रतिकूलः अभवत्। अध्ययनेन स्व-संयोजक-रञ्जक-अणुषु जलीकरणे भीडस्य प्रभावः प्रकाशितः ये तेषां ओलिगोमेराइजेशनं प्रभावितं कुर्वन्ति। गहनतरं अन्वेषणं प्राप्तुं, वयं किर्कवुड-बफ-सिद्धान्ताधारित-अनुकरण-प्रयोगयोः (अस्माकं सहका-रिभिः कृते) द्वयोः अपि, क्राउडर-रञ्जकयोः मध्ये प्राधान्य-अन्तर्क्रियाणां परिमाणं निर्धारयितुं सैद्धान्तिकरूपरेखां परिष्कृतवन्तः। तदनन्तरं अध्ययने वयं सामान्यजलभक्षकरेखीयशाखाबहुल-कानाम् पतनसन्तुलनस्य उपरि मॉडलचार्जित-आणविक-क्राउडर-विभेदक-प्रभावानाम् परी-क्षणं कृतवन्तः। पुनः बहुलकजलीकरणस्य महत्त्वपूर्णा भूमिका इति ज्ञातम्। दुर्बलतया जलयुक्ताः आयनानि रेखीय-शाखायुक्त-बहुलकयोः मध्ये भेदं कुर्वन्ति इति ज्ञातम्, येन पृष्ठसक्रिय-सदृश-तन्त्रेण शाखायुक्त-बहुलकानाम् पतनं भवति। एते क्राउडराः बहुलकस्य मेरुदण्डस्य पार्श्वशृङ्ख-लायाः च सह महत्त्वपूर्णतया अन्तरक्रियां कृतवन्तः, येन पार्श्वशृङ्खलानां मेरुदण्डस्य च परितः जलीकरणजलस्य संरचना भिन्नप्रमाणेन बाधितवती, येन रेखीयशाखायुक्तबहुलकानाम् पतन-स्य भिन्नाः प्रवृत्तयः अभवन्। अन्ते, अस्माभिः एतेषां निष्कर्षाणां प्रमाणीकरणार्थं 16-अवशेष β -हेयरपिनपेप्टाइडस्य संरचनात्मकप्राथमिकतासु आभारित-क्राउडर-प्रभावेषु अस्माकं अन्वे-षणं विस्तारितम्। आदर्श आयनिक-क्राउडर-इत्यनेन पृष्ठसक्रिय-सदृश-तन्त्रेण अधिकाणि पति-तानि गैर-देशीय-पेप्टाइड-संरचनानि प्रवर्धितानि, येन पेप्टाइड-अवस्थानां अनफोल्ड-समूहस्य आभारित-आणविक-क्राउडर-प्रकारस्य प्रति संवेदनशीलतां सूचयति परन्तु कथियनिक-अनायनिक-

क्राउडराः न प्राप्ताः पेप्टाइडस्य गुटितसमूहं महत्त्वपूर्णतया प्रभावितं कर्तुं। समग्रतया अस्मिन् शोधप्रबन्धे प्राप्ताः परिणामाः जैव-आणविक-उपरि आणविक-सङ्केत-प्रभावानाम् उदयमान-दृष्टिकोणं रेखांकयन्ति संरचना स्वसभा च। निष्कर्षाः प्रकाशयन्ति यत् जैव-आणविक-पतनस्य प्रभावं ज्ञातुं भीड-प्रणालीषु मृदु-आकर्षक-अन्तर्क्रियाणां लेखाकरणस्य आवश्यकता वर्तते। कार्येण अपि दर्शितं यत् आकर्षकं सह आणविक-सङ्घटनम् अन्तरक्रियाः रञ्जकानां अल्पसंख्य-कीकरणं प्रतिकूलं कर्तुं शक्नुवन्ति। यत्र, आधारित-आणविक-क्राउडराः बहुलक-वास्तुकलायां भेदं कृत्वा बहुलकानाम् परितः जलीकरण-संरचनायाः आधारेण तेषां पतनस्य नियमनं कर्तुं शक्नुवन्ति। निष्कर्षाणां निहितार्थाः सन्ति यत् आन्तरिकरूपेण अव्यवस्थितप्रोटीनानां मुक्त ऊर्जा परिदृश्यानां आकारं दातुं भीडस्य भूमिका, जैव अणुनां द्रव-द्रवचरणपृथक्करणाय आधारित-भीड-वातावरणानां कृते तथा च अनुरूप-अनुप्रयोगानाम् कृते प्रतिक्रियाशील-बहुलक-आधारित-सामग्रीणां डिजाइनं कर्तुं च।

सार

कोशिका के भीतर का वातावरण, न्यूक्लिक एसिड, प्रोटीन, पॉलीसैकेराइड और छोटे मेटाबोला-इट्स जैसे सघन रूप से पैक किए गए जैव-अणुओं की उच्च सांद्रता (300-400 ग्राम/लीटर) के कारण "भीड़भाड़ वाला" माना जाता है। प्रोटीन बलन जैसी प्रक्रियाओं की ऊष्मागतिकी और गतिकी पर भीड़ भरे वातावरण के प्रभाव को तेजी से पहचाना जा रहा है। भीड़ के सुस्थापित प्रभावों में उनके आकार के कारण भीड़ के एन्ट्रोपिक बहिष्कृत आयतन प्रभावों के कारण जैव-अणुओं का संघनन शामिल है। हालाँकि, हाल की जाँचों ने ऐसी जटिल प्रणालियों में नरम, ऊर्जावान अंतःक्रियाओं के महत्व का संकेत दिया है। इसलिए, इन प्रभावों की व्यापक सूक्ष्म समझ अभी भी अप्राप्य है। इस थीसिस में, हमने आणविक गतिशीलता सिमुलेशन का उपयोग करके मैक्रोमोलेक्यूल्स के स्व-संयोजन और पतन पर आणविक भीड़ के प्रभावों का पता लगाया है। इस परिघटना की जांच करने के लिए, सरलीकृत विलेय मॉडलों पर विचार किया गया, जैसे कि कार्बनिक धनायनिक स्यूडोआइसोसायनिन क्लोराइड (पीआईसी) डाई, जो आंतरिक रूप से अव्यवस्थित प्रोटीन के समान तंतु-जैसी संरचनाएं बनाती है, तथा प्रोटीन एकत्रीकरण के बारे में अंतर्दृष्टि प्रदान करती है। यह पाया गया कि आणविक क्राउडर के रूप में एथिलीन ग्लाइकॉल की नरम-आकर्षक, गैर-विशिष्ट अंतःक्रियाएं डाई ऑलिगोमेराइजेशन को प्रतिकूल रूप से प्रभावित करती हैं। डाई-क्राउडर आकर्षक अंतःक्रियाओं ने डाई ऑलिगोमर्स के जल-योजन घनत्व को कम कर दिया, जिसके परिणामस्वरूप ऊर्जावान दंड उत्पन्न हुआ, जिसने क्राउडेड विलयनों में डाई ऑलिगोमेराइजेशन को प्रतिकूल रूप से प्रभावित किया। अध्ययन में स्व-संयोजन डाई अणुओं के जलयोजन पर भीड़ के प्रभावों पर प्रकाश डाला गया, जो उनके ओलिगोमेराइजेशन को प्रभावित करता है। गहन अंतर्दृष्टि प्राप्त करने के लिए, हमने किर्कवुड-बफ सिद्धांत पर आधारित सिमुलेशन और प्रयोग (हमारे सहयोगियों द्वारा किए गए) दोनों से क्राउडर्स और रंगों के बीच अधिमान्य अंतःक्रियाओं को मापने के लिए सैद्धांतिक ढाँचे को परिष्कृत किया। इसके बाद के अध्ययन में, हमने जेनेरिक हाइड्रोफोबिक रैखिक और शाखित पॉलिमर्स के पतन संतुलन पर मॉडल आवेशित आणविक क्राउडर्स के विभेदक प्रभावों की जांच की। एक बार फिर पाया गया कि बहुलक जलयोजन ने महत्वपूर्ण भूमिका निभाई। यह पाया गया कि कमजोर रूप से जलयोजित ऋणायन रैखिक और शाखित बहुलकों के बीच विभेद करते हैं, तथा सर्फैक्टेंट जैसी क्रियाविधि के माध्यम से शाखित बहुलकों के पतन को प्रेरित करते हैं। ये क्राउडर बहुलक की रीढ़ और पार्श्व श्रृंखलाओं दोनों के साथ महत्वपूर्ण रूप से अंतःक्रिया करते हैं, जिससे पार्श्व श्रृंखलाओं और रीढ़ के चारों ओर जलयोजन जल की संरचना विभिन्न स्तरों पर बाधित होती है, जिसके परिणामस्वरूप रैखिक और शाखित बहुलकों के पतन की विभिन्न प्रवृत्तियां उत्पन्न होती हैं। अंत में, हमने इन निष्कर्षों को मान्य करने के लिए 16-अवशेष β -हेयरपिन पेप्टाइड की संरचनात्मक प्राथमिकताओं पर आवेशित क्राउडर्स के प्रभावों पर अपनी जांच को आगे बढ़ाया।

मॉडल एनायनिक क्राउडर्स ने सर्फेक्टेंट-जैसी क्रियाविधि के माध्यम से अधिक संकुचित गैर-देशी पेप्टाइड संरूपणों को बढ़ावा दिया, जो आवेशित आणविक क्राउडर्स के प्रकार के लिए पेप्टाइड अवस्थाओं के अनफोल्डेड समूह की संवेदनशीलता को दर्शाता है। हालाँकि, यह पाया गया कि धनायनिक और ऋणायनिक क्राउडर्स पेप्टाइड के फोल्डेड समूह को महत्वपूर्ण रूप से प्रभावित नहीं करते हैं। कुल मिलाकर, इस थीसिस में प्राप्त परिणाम जैव-आणविक संरचना और स्व-संयोजन पर आणविक भीड़ के प्रभावों के उभरते दृष्टिकोण को रेखांकित करते हैं। निष्कर्ष इस बात पर प्रकाश डालते हैं कि जैव-आणविक पतन पर प्रभाव को समझने के लिए भीड़-भाड़ वाली प्रणालियों में कोमल, आकर्षक अंतःक्रियाओं को ध्यान में रखना आवश्यक है। इस कार्य से यह भी पता चला कि आकर्षक अंतःक्रिया वाले आणविक क्राउडर रंगों के ऑलिगोमियराइजेशन को प्रतिकूल रूप से प्रभावित कर सकते हैं। जबकि, आवेशित आणविक क्राउडर बहुलक संरचना के बीच भेदभाव कर सकते हैं और बहुलकों के चारों ओर जलयोजन संरचना के आधार पर उनके पतन को नियंत्रित कर सकते हैं। इन निष्कर्षों में आंतरिक रूप से अव्यवस्थित प्रोटीनों के मुक्त ऊर्जा परिदृश्यों को आकार देने, जैव-अणुओं के द्रव-द्रव प्रावस्था पृथक्करण के लिए आवेशित भीड़ भरे वातावरण और अनुरूप अनुप्रयोगों के लिए उत्तरदायी बहुलक-आधारित सामग्रियों को डिजाइन करने में भीड़ की भूमिका के निहितार्थ हैं।

Abstract

Intracellular environment is considered as crowded due to the high concentrations (300 – 400 g/L) of tightly packed biomolecules such as nucleic acids, proteins, polysaccharides and small metabolites. The impact of crowded milieu on thermodynamics and kinetics of the processes like protein folding is being increasingly recognized. The well-established effects of crowding include the compaction of biomolecules caused by entropic excluded volume effects of crowders due to their size. Recent investigations, however, have indicated the significance of the soft, energetic interactions in such complex systems. Therefore, a comprehensive microscopic understanding of these effects remains elusive. In this thesis, we have explored the effects of molecular crowding on the self-assembly and collapse of macromolecules using molecular dynamics simulations. To investigate this phenomena, simplified solute models were considered, such as the organic cationic pseudoisocyanine chloride (PIC) dye, which forms fibril-like structures similar to intrinsically disordered proteins, offering insights into protein aggregation. It was found that the soft-attractive, non-specific interactions of ethylene glycol as a molecular crowder disfavoured dye oligomerization. The dye-crowder attractive interactions reduced the hydration density of dye oligomers, leading to an energetic penalty that disfavoured dye oligomerization in crowded solutions. The study highlighted the effects of crowding on the hydration of the self-assembling dye molecules that influence their oligomerization. To gain a deeper insights, we refined the theoretical framework to quantify the preferential interactions between crowders and dyes, from both simulations and experiments (performed by our collaborators) based on Kirkwood-Buff theory. In the subsequent study, we examined the differential effects of model charged molecular crowders on the collapse equilibria of generic hydrophobic linear and branched polymers. It was once again found that the polymer hydration played a crucial role. Weakly hydrated anions were found to discriminate between linear and branched polymers, inducing the collapse of branched polymers through a surfactant-like mechanism. These crowders interacted significantly with both the backbone and side chains of the polymer, disrupting the structure of hydration waters around the side-chains and backbone to different extents, leading to different propensities of collapse of linear and branched polymers. Finally, we extended our investigation into the effects of charged crowders on the structural preferences of a 16-residue

β -hairpin peptide to validate these findings. The model anionic crowders promoted more collapsed non-native peptide conformations via surfactant-like mechanism, indicating the sensitivity of the unfolded ensemble of the peptide states to the type of charged molecular crowders. However, the cationic and anionic crowders were found not to significantly affect the folded ensemble of the peptide. Overall, the results obtained in this thesis underscore the emerging view of molecular crowding effects on biomolecular structure and self-assembly. The findings highlight that soft, attractive interactions in crowded systems need to be accounted for in order to understand the effects on biomolecular collapse. The work also showed that molecular crowders with attractive interactions can disfavour oligomerization of dyes. Whereas, the charged molecular crowders can discriminate between polymer architecture and regulate their collapse based on the hydration structure around the polymers. The findings have implications for the role of crowding in shaping the free energy landscapes of intrinsically disordered proteins, charged crowded environments for liquid-liquid phase separation of biomolecules and for designing responsive polymer-based materials for tailored applications.

Permissions

Permissions have been taken from the respective journals for the publications related to the work presented in this thesis.

List of Publications Related to Work Presented in this Thesis as of Date of Submission of Thesis.

1. **S. Rajput**, R. Pollak, K. Huber, S. Ebbinghaus, D. Nayar, "Ethylene glycol energetically disfavours oligomerization of pseudoisocyanine dyestuffs at crowded concentrations", *Soft Matter*, 2023, **19**, 6399 – 6413.
2. **S. Rajput**, D. Nayar, "Effects of polymer architecture and charged molecular crowders on hydrophobic polymer collapse", *ACS Polym. Au* 2024, **4**, 289-301.
3. **S. Rajput**, Sibasankar Panigrahy, D. Nayar, "In silico view of crowding: Biomolecular processes to nanomaterial design", *ACS Omega*, 2024, **9**, 28, 29953 – 29965.
4. L. Koch, **S. Rajput**, D. Nayar, S. Ebbinghaus, K. Huber, *Self-Assembly of Pseudo Isocyanine Chloride in the Presence of Attractive Polyethylene Glycol Crowders. J. Phys. Chem. B*, 2025.
5. **S. Rajput**, D. Nayar *Anionic Crowders Strongly Influence β -Hairpin Peptide Unfolded Conformations Crowders Impact on β -Hairpin Structure. (Under Peer-review)*

Contents

Certificate	i
Acknowledgments	viii
संक्षेपः	xi
सार	xiii
Abstract	xv
Permissions	xix
LIST OF TABLES	xxv
LIST OF FIGURES	xl
ABBREVIATIONS	xli
NOTATION	xlii
1 Introduction	1
1.1 Cellular Environments: The Crowded Soup	1
1.2 Role of Excluded Volume Effects in Biomolecular Processes: Traditional View	4
1.3 Non-specific attractive interactions: Emerging View	12
1.4 The Computational Lens: Simulating Crowding Effects	17
1.5 Gaps in understanding	23
1.5.1 Objectives of the Thesis	25
1.5.2 Organisation of the Thesis	25

2	Computational Methods and Solvation Theory	29
2.1	The Born-Oppenheimer Approximation and Molecular Simulation	29
2.1.1	Classical behaviour of particles	31
2.2	Force field or Potential energy function in Molecular Mechanics	32
2.2.1	Bonded potential energy	33
2.2.2	Non-bonded potential energy	33
2.3	Molecular Dynamics: A Window into the Microscopic World .	35
2.3.1	Numerical integration algorithms	36
2.3.2	Time step in numerical integration	39
2.3.3	Temperature and Pressure coupling	39
2.4	Enhanced Sampling Methods	43
2.4.1	Umbrella Sampling Method	44
2.5	From Microscopic Interactions to Macroscopic Properties: Kirkwood-Buff Integrals from Molecular Simulations	50
2.6	Widom potential distribution theorem	53
2.6.1	Widom potential distribution	54
2.6.2	Unravelling the solvation thermodynamics: Exploring the process and understanding the solute-solvent interaction	56
2.6.3	Exploring the pseudo-chemical potential	58
3	Effects of Ethylene Glycol as a Molecular Crowder on Oligomerization of Pseudoisocyanine Chloride Dye-stuffs	61
3.1	Introduction	61
3.2	Theory	69
3.3	Computational details	71
3.4	Results and Discussion	75
3.5	Conclusions	95
4	Preferential Interactions of Ethylene Glycol with Pseudoisocyanine Chloride Dye-stuff inhibits Self-assembly: A Combined Theory, Simulations, and Experimental Study	98
4.1	Introduction	98
4.2	Theoretical Approach	101
4.2.1	Determination of the derivatives of the chemical potential μ_{23} through experiments	101

4.2.2	Determination of the derivatives of the chemical potential μ_{23} using Kirkwood-Buff theory through molecular simulations	102
4.3	Computational Methodology	107
4.3.1	System setup	107
4.3.2	Simulation details	107
4.4	Computation of a_{33} and Γ_{23}	109
4.4.1	Computation of activity coefficient of EG using corrected KBIs	109
4.4.2	Temp. dependence of KBIs for computing a_{33}	110
4.4.3	Computation of Γ_{23} at different temperature	110
4.5	Results and Discussion	113
4.5.1	Determination of crowder concentration on dependence of μ_{23} using Molecular Dynamics	114
4.5.2	Determination of temperature dependence of μ_{23} in EG solution	115
4.6	Determination of crowder degree of polymerization dependence of μ_{23}	118
4.7	Conclusions	120
5	Role of Polymer Architecture and Charged Molecular Crowders in Determining Hydrophobic Polymer Collapse	128
5.1	Introduction	128
5.2	Computational Methods	132
5.2.1	Solvation Thermodynamics	132
5.2.2	System Setup	133
5.2.3	Simulations Details	134
5.2.4	Umbrella Sampling Simulations	135
5.2.5	Simulations for Computing Energetics and Observables	137
5.3	Results	138
5.3.1	Polymer Collapse Equilibria in Pure Water	138
5.3.2	Polymer Collapse Equilibria in Charged Molecular Crowder Solutions	142
5.4	Discussion and Conclusions	151
6	Effect of Charged Crowders on Folded and Unfolded Ensembles of β-hairpin Peptide	155
6.1	Introduction	155

6.2	Computational Methods	157
6.2.1	System Setup	157
6.2.2	Simulation details	158
6.3	Observables	159
6.3.1	Radius of gyration (R_g)	159
6.3.2	Root Mean Square Deviation (RMSD)	160
6.3.3	Ramachandran plot	160
6.3.4	Preferential Binding Coefficient	161
6.4	Results and Discussion	162
6.4.1	Crowding effects on hydrophobic core of the peptide . .	162
6.4.2	Residue-specific interactions of peptide with crowders .	165
6.4.3	Discussion and Conclusions	169

7 Conclusions **171**

List of Tables

3.1	The table provides details about the system setup. Here, $\langle l \rangle$ represents the average box length in nanometers (nm), $\langle \rho \rangle$ denotes the average solution density in g cm^{-3} , and N_w and N_c indicate the respective number of water molecules and crowders within the system.	74
3.2	The binding free energy ($\Delta G^{u \rightarrow b}$), the change in dye-solvent entropy ($\Delta S^{u \rightarrow b} dv$), and the energy ($\Delta E^{u \rightarrow b} dv$) associated with the oligomerization of H- and J-oligomers are presented. All energy values are expressed in kJ mol^{-1} . The symbols w and c in parentheses represent pure water and crowded solution, respectively.	87
3.3	The interaction energy changes for dyewater ($\Delta E_{dw}^{u \rightarrow b}$), dye-crowder ($\Delta E_{dc}^{u \rightarrow b}$), dyedye ($\Delta E_{dd}^{u \rightarrow b}$), and dyeion ($\Delta E_{di}^{u \rightarrow b}$) contribute to the total dyesolvent energy change ($\Delta E_{dv}^{u \rightarrow b}$). All energy values are expressed in kJ mol^{-1}	88
3.4	The interaction energies between different components in aqueous solutions of dispersed PIC dye molecules in aqueous crowded solution of ethylene glycol. Here, E_{dw} is dye-water, E_{dc} is dye-crowder, E_{dd} is dye-dye, E_{di} dye-ion, E_{ww} is water-water, E_{cc} is crowder-crowder, E_{cw} is crowder-water interaction energy in kJ/mol . To compute this data, separate MD simulations were performed with one to five PIC monomers dispersed in aqueous ethylene glycol with no oligomers in solution. The simulation parameters used remain the same as described in the Methods section of the main manuscript.	94

-
- 4.1 The details of the simulated systems included 4 mM PIC in the presence of varying concentrations of ethylene glycol. For each system, the ethylene glycol concentration is expressed both in g/L and in mol/L (c_3). The parameter $\langle l \rangle$ represents the average box length, N_{eg} indicates the number of ethylene glycol molecules, N_w specifies the number of water molecules, and $\langle \rho \rangle$ refers to the system's average density. 109
- 4.2 Averaged values of μ_{23} and the corresponding number of $\delta \ln m_{2,ss}/m_3$ for EG/PEG-based crowding agents at variable degree of polymerization DP of the crowder samples. ^[a]From Hämisch et al.¹³. 127
- 4.3 The standard enthalpy ΔH^0 , the standard entropy ΔS^0 , and the standard Gibbs energy ΔG^0 of J-aggregate formation in the presence of EG, PEG 600 and PEG 1000 established by means of eq 10 for all three crowder samples at four crowder concentrations, respectively. 127
- 5.1 Details of each system for hydrophobic Poly-I and Poly-II polymers in conjunction with 330 charged crowders. Where ϕ , N_w , and N_c represent the packing fraction in %, the number of water molecules, and the crowders involved in the system, respectively. $\langle l \rangle$ and $\langle \rho \rangle$ represent the average side length of the box in nanometers and the average density of the system in $g\ cm^{-3}$, obtained from the simulations. 134
- 6.1 The details of each conformation are provided. Here, end to end termini distance is (R_{ee} in nm), radius of gyration is (R_g in nm), and number of the crowders are represented with (N_c). The conformation F represents the folded state, while the unfolded conformations are represented by I_1 , I_2 , and I_3 . . 159

List of Figures

1.1	Artist David Goodsell's depiction of a cross-sectional view of an Escherichia coli cell. At the top, the cell wall is depicted. The middle section represents the cytoplasm, which contains soluble proteins, RNA, ribosomes, and proteasomes. The bottom part illustrates the nucleoid interior, characterised by a high concentration of DNA and DNA-binding proteins. Reprinted with permission from ref. [16] Copyright 2009 Wiley.	2
1.2	The picture illustrates the differences between the <i>in vitro</i> and <i>in vivo</i> environments. Reprinted under the terms of the Creative Commons Attribution License from ref. [20] has been adapted from ref. [21].	3
1.3	Two hard spheres are immersed in a medium containing penetrable hard spheres (PHS) acting as depletants. These depletants exert an unbalanced osmotic pressure, P , on the hard spheres, resulting in a depletion attraction between them. The blue dotted lines surrounding the peach-colored spheres (hard spheres) represent the depletion layers in the illustration. The overlap volume of these layers, shown as a lens-shaped region, is highlighted with a width h . Additionally, the figure includes some key notations: σ , representing the diameter of the penetrable hard spheres; R , the radius of the hard spheres; P , the osmotic pressure; and θ_0 , the angle between the osmotic pressure and the x-axis. Reprinted under the terms of the Creative Commons Attribution License from ref [36].	6

-
- 1.4 Thermodynamic cycle illustrating the free energy change during the association of biomolecules in dilute and crowded environments, and the transfer of reactants and products from a dilute solution to a crowded medium. Reprinted with permission from ref. [6] Copyright 2008 Annual Reviews. 8
- 1.5 (a) The cartoon illustration represents a living cell with a crowded cytoplasm and several molecules constituting the heterogeneous crowded soup. Adapted from ref. [21] Copyright Garland Science 2012. (b) The right panel presents a schematic of the traditional view of macromolecular folding-unfolding equilibria (top) and nanomaterial self-assembly (bottom), highlighting volume exclusion effects and depletion attraction. Reprinted with permission from ref. [52] Copyright 2016 Elsevier Ltd. In contrast, the left panel illustrates the overlap in excluded volumes during biomolecular collapse, aggregation, helix formation, etc. Reprinted with permission from ref. [7] Copyright 2006 The Rockefeller University Press. The bottom-most figure depicts the Asakura-Oosawa theory, which explains colloidal aggregation in a solution of polymers (this figure has been discussed at the beginning of the section). Reprinted with permission from ref. [34] Copyright 2021 AIP Publishing. (c) The emerging view incorporates enthalpic interactions via the preferential adsorption of crowders. The left panel demonstrates the direct preferential interactions of crowders with biomolecules. Reprinted with permission from ref. [52] Copyright 2016 Elsevier Ltd. Additionally, the right panel summarises the thermodynamic forces in an enthalpy-entropy plot for various crowders. The schematic at the bottom highlights both the solvent-mediated enthalpic mechanism and the volume-exclusion entropically stabilising mechanism. Reprinted with permission from ref. [53] Copyright 2013 Elsevier Ltd., and the full image is reprinted under the terms of the Creative Commons Attribution License from ref [20]. 10

- 1.6 (A) The picture shows the proto-fibrillation of the A β 40 peptide in the presence of mannose, an electron microscopy image. Reprinted with permission from ref. [44] Copyright 2005 Elsevier. (B) The image depicts the free-energy profile as a function of the radius of gyration of the monomer within the dimer at various packing fractions (ϕ_C) values. Reprinted with permission from ref. [45] Copyright 2011 American Chemical Society. (C) The image illustrates the number of peptides in fibrils as a function of reduced time for a crowder size of 5 Å. The green colour represents a packing fraction (ϕ) of crowd-ers equal to 0, the orange colour corresponds to $\phi = 0.10$, and the purple colour indicates $\phi = 0.20$. Reprinted with permission from ref. [46] Copyright 2015 Biophysical Society. 11
- 1.7 This picture illustrates the historical development of the macro-molecular crowding (MMC) effects. Images (from top to bot-tom) reprinted with permission from: ref. [34], Copyright 2021 AIP Publishing; ref. [43], Copyright 1981 American Chemical Society; ref. [67], Copyright 1994 AIP Publishing; ref. [49], Copyright 2022 Annual Reviews; and ref. [61], Copyright 2014 American Chemical Society. 14
- 1.8 (A) The image depicts an entropy-enthalpy plot illustrating the effects of polymeric crowd-ers on various protein processes. In this representation, different colours indicate the identity of the crowd-ers, while the symbol shapes correspond to spe-cific proteins and their respective processes. Reprinted with permission from ref. [53] Copyright 2013 Elsevier. (B) The image illustrates the excess free energy of ubiquitin unfold-ing ($\Delta\Delta G_u$) as a function of the volume fraction of glucose. Reprinted with permission from ref. [61] Copyright 2014 Amer-ican Chemical Society. (C) The image depicts the time-dependent diffusion coefficient of Ficoll70 along the x-axis for the three analysed systems. D_0 represents the diffusion coefficient of Ficoll70 in infinite dilution in water or in the absence of crowd-ers. The occupied volume fraction is $\phi_{\text{occ}} = 5\%$, and the molar fraction of dsDNA is $x_{\text{DNA}} = 25\%$. Reprinted with permission from ref. [69] Copyright 2020 American Chemical Society. 16

- 1.9 The picture illustrates the investigation of crowding effects *in silico* and *in vitro*. (A) The snapshots show the crowded protein-G system (PG4) and the protein-G/villin headpiece protein system (PGVH5), the anomalous mean square displacement of water as a function of time for the PGVH5 system, the decrease in the dielectric constant of water with increasing protein volume fractions, and the decrease in water dipole autocorrelation over time (in ps). All sub-images have been reprinted with permission from ref. [57] Copyright 2012 American Chemical Society. (B) The first and second images represent the associated water dynamics, which become flexible at low concentrations of Ficoll-70 and rigid at higher concentrations. The third image represents the comparison of the average solvation time as a function of Ficoll-70 concentration. Finally, the differential entropic component, $-\Delta\Delta S = -T(\Delta S_{\text{Ficoll}} - \Delta S_{\text{buffer}})$ for the thermal stabilisation of bromelain in the presence of different concentrations of Ficoll-70 is shown. All sub-images have been reprinted with permission from ref. [101] Copyright 2023 Wiley. 22
- 2.1 The typical flowchart of an MD simulation. 37
- 2.2 Schematic representation of the Umbrella Sampling (US) method. The x-axis represents the reaction coordinate (ξ), while the y-axis denotes the biased potential energy ($\omega(\xi)$). The grey curve exhibits the free energy profile, which contains high-energy barriers. The red parabolic curves represent harmonic biasing potentials applied at different windows (ξ_0) along the reaction coordinate, indicated by red markers. The blue dashed lines indicate the boundaries of individual sampling windows. 46
- 2.3 A schematic representation of a radial shell within a binary mixture composed of two types of particles, labelled as type i and type j . The radial distribution function, $g_{ij}(r)$, is determined by calculating the distance from an i -type particle to a j -type particles, with incremental steps of dr . The radius of the shell is defined as R , representing the boundary at which the radial distribution is measured. Reprinted with permission from ref. [183] Copyright 2013 American Chemical Society. 50

-
- 2.4 The definition of the solvation process where a spherical solute (s) is going to transfer from the fixed position in the ideal-gas phase to the fixed position in the liquid phase. 57
- 3.1 The picture depicts the chemical structure of pseudoisocyanine chloride (PIC) dye. 63
- 3.2 This image illustrates the schematic representation of changes in the absorption (blue) and fluorescence (red) spectra during the formation of H- and J-aggregates from cyanine dye monomers. Reprinted under the terms of the Creative Commons Attribution License from ref. [119]. 64
- 3.3 The exciton model proposed by Michael Kasha explains how the energy levels of molecular dimers change during electronic transitions. In H-type dimers, where the molecules associate side-by-side or on top of each-other, the energy separation between the absorbing and emitting states is significantly increased. This configuration often results in weak fluorescence due to the forbidden nature of these transitions. On the other hand, in J-type dimers, where one quiniline ring is on top of the other, the transition dipoles are aligned linearly. This alignment causes a substantial reduction in transition energy and an increase in the transition dipole moment, leading to enhanced light absorption. Additionally, J-type dimers exhibit red-shifted absorption and emission spectra, though these shifts do not necessarily reflect changes in energy differences between states. Reprinted under the terms of the Creative Commons Attribution License from ref [119]. 66
- 3.4 The picture shows the bound (a,c) state in H- and J-conformations, respectively, and unbound (b,d) states in H- and J-conformations. Reprinted with permission from ref. [212] Copyright 2023 Royal Society of Chemistry. 67
- 3.5 The image represents the large size oligomer (dodecamer) in H- and J-conformation. 68

- 3.6 The image (a) represents the schematic diagram depicting the free energy of solvation of dye molecules. Where $\Delta G(r)$ is the free energy of the pair of oligomers in unbound state where monomer is fixed at the r nm distance from $(n - 1)^{th}$ -mer oligomer. (b) represents the thermodynamic cycle which involves the association of dye molecules in pure water as well as in aqueous ethylene glycol crowded solutions. Here, $\Delta G^{u \rightarrow b}(w)$ represents free energy of association in pure-water and $\Delta G^{u \rightarrow b}(c)$ in crowded environment. Reprinted with permission from ref. [212] Copyright 2023 Royal Society of Chemistry. 69
- 3.7 Radial distribution functions for crowder-water and crowder-crowder interactions in solutions containing (a, b) H-oligomers and (c, d) J-oligomers. Reprinted with permission from the supplementary information (SI) of ref. [212] Copyright 2023 Royal Society of Chemistry. 73
- 3.8 The radial distribution function (RDF) of the center of mass for dye-dye interactions is shown for the H-aggregate in (a) pure water and (b) aqueous ethylene glycol, and for the J-aggregate in (c) pure water and (d) aqueous ethylene glycol. Reprinted with permission from the supplementary information (SI) of ref. [212] Copyright 2023 Royal Society of Chemistry. 76
- 3.9 The radial distribution functions (RDFs) for dyecrowder (a, b) and dyewater (c, d) interactions are shown for H- and J-aggregates (12-mer) in an aqueous ethylene glycol solution. Panels (c) and (d) display the dyewater RDFs for H- and J-aggregates in both pure water and the crowded solution. The black curves represent the RDFs for a system with 12 dispersed PIC monomers, where no aggregation occurs. The snapshots at the top illustrate the H-aggregate (left) and J-aggregate (right) structures. Reprinted with permission from ref. [212] Copyright 2023 Royal Society of Chemistry. 77

- 3.10 The image shows the potentials of mean force (PMF), $w(r)$ in-y-axis, as a function of r , which is the center of mass distance between oligomers $(n - 1)^{th}$ -mer and monomer n^{th} dye, in (a) pure-water (b) aqueous ethylene glycol solutions) for H-oligomer and (c,d) represent in pure water and aqueous ethylene glycol solutions for J-oligomers, respectively. The numbers in parentheses represent the local minima in the PMF profiles, with corresponding snapshots. Reprinted with permission from ref. [212] Copyright 2023 Royal Society of Chemistry. 78
- 3.11 The binding free-energy ($\Delta G^{u \rightarrow b}$) as a function of oligomer size for (a) H and (b) J-oligomers. Reprinted with permission from ref. [212] Copyright 2023 Royal Society of Chemistry. . . 79
- 3.12 Snapshots of PIC H-oligomers: 1 (a) tetramer in pure water at its global minimum of 0.82 nm. (2) Tetramer in aqueous ethylene glycol at (a) the first local minimum of 0.72 nm, (b) the global minimum of 0.82 nm, and (c) the second local minimum of 0.92 nm. (3) Pentamer in pure water at (a) the first local minimum of 0.62 nm, (b) the second local minimum of 0.74 nm, and (c) the global minimum of 1.05 nm. (4) Pentamer in aqueous ethylene glycol at (a) the first local minimum of 0.62 nm, (b) the second local minimum of 0.74 nm, and (c) the global minimum of 1.05 nm. Reprinted with permission from the supplementary information (SI) of ref. [212] Copyright 2023 Royal Society of Chemistry. 81
- 3.13 Snapshots of PIC J-oligomers: (1) Trimer in pure water at (a) a local minimum of 0.72 nm and (b) a global minimum of 1.05 nm. (2) Trimer in aqueous ethylene glycol at (a) a local minimum of 0.82 nm and (b) a global minimum of 1.02 nm. (3) Tetramer in (a) pure water at a global minimum of 1.05 nm and (b) aqueous ethylene glycol at a global minimum of 1.05 nm. (4) Pentamer in (a) pure water at a global minimum of 1.12 nm and (b) aqueous ethylene glycol at a global minimum of 1.12 nm. Reprinted with permission from the supplementary information (SI) of ref. [212] Copyright 2023 Royal Society of Chemistry. 82

- 3.14 The preferential binding coefficient (Γ) of crowders on (a) H-oligomer and (b) J-oligomers. Reprinted with permission from ref.[212] Copyright 2023 Royal Society of Chemistry. 83
- 3.15 The profiles of binding free energy ($\Delta G^{u \rightarrow b}$), change in dye-solvent energy ($\Delta E^{u \rightarrow b}$), and change in dye-solvent entropy ($\Delta S^{u \rightarrow b}$) during dye association into H-oligomers are presented. The left column corresponds to pure water solutions, while the right column represents aqueous ethylene glycol solutions. Reprinted with permission from the supplementary information (SI) of ref. [212] Copyright 2023 Royal Society of Chemistry. 84
- 3.16 Profiles of the components of the total dye-solvent energy change ($\Delta E_{u \rightarrow b}$) for H-oligomers, including contributions from the change in dye-water energy ($\Delta E_{u \rightarrow b}^{dw}$), dye-dye energy ($\Delta E_{u \rightarrow b}^{dd}$), and dye-crowder energy ($\Delta E_{u \rightarrow b}^{dc}$), which also accounts for dye-ion interactions, are presented. The left column corresponds to pure water solutions, while the right column represents aqueous ethylene glycol solutions. Reprinted with permission from the supplementary information (SI) of ref.[212] Copyright 2023 Royal Society of Chemistry. 85
- 3.17 The dye-solvent energy ($\Delta E_{dv}^{u \rightarrow b}$) and entropy change ($-T\Delta S_{dv}^{u \rightarrow b}$) on dye-association for H-oligomers in (a) pure water, (b) aqueous ethylene glycol solution. While parts (c, d) representing the decomposition of total energy ($\Delta E_{dv}^{u \rightarrow b}$) in pure-water and aqueous ethylene glycol solution respectively, arises from changes in dyewater interaction energy ($\Delta E_{dw}^{u \rightarrow b}$) and dyedye interaction energy ($\Delta E_{dd}^{u \rightarrow b}$), which also encompasses dyeion and dyecrowder interaction energies ($\Delta E_{dc}^{u \rightarrow b}$). Reprinted with permission from ref. [212] Copyright 2023 Royal Society of Chemistry. 86
- 3.18 The profiles of binding free energy ($\Delta G_{u \rightarrow b}$), change in dye-solvent energy ($\Delta E_{u \rightarrow b}$), and change in dye-solvent entropy ($\Delta S_{u \rightarrow b}$) during dye association into J-oligomers are presented. The left column corresponds to pure water solutions, while the right column represents aqueous ethylene glycol solutions. Reprinted with permission from the supplementary information (SI) of ref. [212] Copyright 2023 Royal Society of Chemistry. 89

- 3.19 Profiles of the components of the total dye-solvent energy change ($\Delta E_{u \rightarrow b}$) for J-oligomers, including contributions from the change in dye-water energy ($\Delta E_{u \rightarrow b}^{dw}$), dye-dye energy ($\Delta E_{u \rightarrow b}^{dd}$), and dye-crowder energy ($\Delta E_{u \rightarrow b}^{dc}$), which also accounts for dye-ion interactions, are presented. The left column corresponds to pure water solutions, while the right column represents aqueous ethylene glycol solutions. Reprinted with permission from the supplementary information (SI) of ref. [212] Copyright 2023 Royal Society of Chemistry. 90
- 3.20 The dye-solvent energy ($\Delta E_{dv}^{u \rightarrow b}$) and entropy change ($-T \Delta S_{dv}^{u \rightarrow b}$) on dye-association for J-oligomers in (a) pure water, (b) aqueous ethylene glycol solution. While parts (c, d) represents the decomposition of total energy ($\Delta E_{dv}^{u \rightarrow b}$) in pure-water and aqueous ethylene glycol solution respectively, arises from changes in dyewater interaction energy ($\Delta E_{dw}^{u \rightarrow b}$) and dyedye interaction energy ($\Delta E_{dd}^{u \rightarrow b}$), which also encompasses dyeion and dye-crowder interaction energies ($\Delta E_{dc}^{u \rightarrow b}$). Reprinted with permission from ref. [212] Copyright 2023 Royal Society of Chemistry. 91
- 3.21 The ITC experiments reveal the resulting ΔH_m values for PIC/EG interactions under two conditions: (a) 2 mM PIC with 40 mM ethylene glycol (EG) and (b) 2 mM PIC with 100 mM EG. The molar ratio represents the concentration of EG relative to PIC. The insets illustrate the DP values obtained from titrating EG into the PIC solution (black), EG into water (red), and water into the PIC solution (blue). Typically, DP decreases at the equilibrium point due to dilution; however, in this case, no such reduction occurs, preventing the estimation of the Gibbs energy of mixing, mixing entropy, or association constant through fitting. Error bars reflect the standard deviation derived from three independent measurements. Reprinted with permission from ref. [212] Copyright 2023 Royal Society of Chemistry. 93

- 3.22 The schematic represents the molecular mechanisms underlying the oligomerisation of (a) H-oligomers and (b) J-oligomers. The blue colour around the dyes represents the water density in their solvation shells. In the bound state of oligomers, the dyewater interaction is energetically favourable due to the high charge density. However, in crowded environments, ethylene glycol tends to adsorb on dye oligomers, resulting in a more favourable dyecrowder interaction in the unbound state. This interaction hinders dye association and renders the binding free energy of J-oligomers unfavourable in crowded conditions compared to pure water. For H-oligomers, dyedye repulsions in the bound state contribute to an unfavourable change in total dyesolvent energy. The arrows in the schematic indicate the relative contribution of dyesolvent energy changes, with short arrows representing weaker contributions and long arrows representing stronger ones. Reprinted with permission from ref. [212] Copyright 2023 Royal Society of Chemistry. . . 97
- 4.1 The image represents the packed system with 0.486 M concentration of ethylene glycol as crowders in a 12 nm cubical box length. The six PIC dyes are in a dispersed state, and yellow spheres represent the counterions in the solutions. Water molecules have not been shown for clarity in the picture. . . . 107
- 4.2 Evaluation of the correction method (Ref. 7) applied to the radial distribution function (RDF) is shown for (a) EG-EG and (c) EG-water pair interactions in an aqueous solution of 1.788 M EG (without PIC). Various correction approaches for Kirkwood-Buff integrals (KBI) are applied to improve tail convergence, as presented for (b) EG-EG and (d) EG-water interactions (Refs. 8, 9). The methods include the running uncorrected KBI (**R-KBI**), KBI derived from corrected RDF (**G-KBI**), KBI with direct correction (**K-KBI**), and KBI with corrections applied to both the KBI and RDF (**B-KBI**) (Ref. 9). Additionally, the derivative of the activity coefficient of EG ($a_{\text{EG-EG}}$) is compared for PIC-water-EG solutions with 4 mM and 8 mM PIC concentrations against a binary EG-water mixture at (e) 275 K and, (f) 275 K and 285 K. . . 111

- 4.3 The corrected Kirkwood-Buff integrals (B-KBI) for EG-water (G_{13}) interactions are presented in the left column, while those for EG-EG (G_{33}) interactions are shown in the right column. These values were obtained for PIC solutions containing varying concentrations of EG and at different temperatures. In this context, components 1, 2, and 3 correspond to water, the PIC dye, and EG, respectively. 112
- 4.4 The preferential binding coefficient of EG (Γ_{23}) on the dye surface is depicted as a function of the proximal distance (r_p) from the dye surface for PIC aqueous solutions at various EG concentrations and temperatures. The shaded regions indicate the corresponding error margins. 113
- 4.5 (a) The positive values of preferential binding coefficient (Γ_{23}) indicate the preferential adsorption of ethylene glycol (3) on surface of PIC (2) (b) the values of quantity, a_{33} , is indicating the solution to become non-ideal on increasing the concentration of ethylene glycol (c) the chemical potential derivative, μ_{23}^M cal mol⁻¹ molar⁻¹, of PIC as a function of EG concentration computed using first approach (A) (d) the relative concentration of PIC in EG solution as a function of EG concentration at various temperatures, computed using second approach. Dotted lines represent simulation data, while solid lines correspond to experimental results. 114
- 4.6 (a) Molal concentrations $m_{2,ss}$ of PIC aggregation threshold as a function of the molar c_3 of the crowder at different temperatures as obtained from experiments. (b) Temperature dependence of the chemical potential derivative μ_{23} for PIC in the presence of ethylene glycol (blue), PEG 600 (black), and PEG 1000 (red) as obtained from experiments. (c) Comparison of chemical potential derivative, μ_{23} , as a function of temperature as obtained from simulations and experiments. 117

4.7	The correlation between the averaged μ_{23} values and the degree of polymerisation (DP) of various EG-based crowding agents, including EG, PEG 600, and PEG 1000 from the present study, as well as TEG and PEG 400 from ref. [210], is presented. This analysis highlights the dependence of μ_{23} on the molecular size and structure of the crowders, providing a comprehensive comparison across the different crowding agents. This data is obtained from experiments.	119
5.1	The study explores generic hydrophobic polymers, including (a) a 50-mer linear polymer referred to as Poly-I and (b) a branched polymer called Poly-II, both examined in aqueous crowded solutions containing (c) charged hydrophobic tetramer molecules, CR+ and CR-. Reprinted under the terms of the Creative Commons Attribution License from ref [105].	136
5.2	The 2D probability distributions are presented for: (a, b) the solvent-accessible surface area (SASA) and radius of gyration (R_g) for Poly-I and Poly-II, respectively, and (c, d) the number of hydrophobic contacts and R_g for Poly-I and Poly-II, respectively, in pure water. Reprinted under the terms of the Creative Commons Attribution License from ref [105].	139
5.3	Potential of mean force ($w(R_g)$) profiles are shown for (a) Poly-I and (b) Poly-II in pure water. The inset in (a) displays the profile for a 32-mer linear polymer, with data obtained from ref. 33. Snapshots illustrate representative polymer conformations at different R_g values. Reprinted under the terms of the Creative Commons Attribution License from ref [105].	140
5.4	The potential of mean force ($w(R_g)$) profiles are shown for (a) Poly-I and (b) Poly-II in aqueous solutions containing anionic and cationic crowders. The snapshots represent polymer conformations at different R_g values. Reprinted under the terms of the Creative Commons Attribution License from ref [105]. The error bars are within the point size.	142
5.5	The collapse free energy ($\Delta G^{E \rightarrow C}$) of Poly-I and Poly-II in aqueous solutions of anionic and cationic crowders. Reprinted under the terms of the Creative Commons Attribution License from ref [105].	143

- 5.6 The preferential binding coefficients are presented for (a, e) CR+, (b, f) CR-, (c, g) Cl⁻, and (d, h) Na⁺ as a function of the proximal distance r from the surface of Poly-I and Poly-II, respectively. Reprinted under the terms of the Creative Commons Attribution License from ref [105]. 144
- 5.7 (a) Changes in the polymer-solvent energy ($\Delta E_{pv}^{E \rightarrow C}$) and entropy ($\Delta S_{pv}^{E \rightarrow C}$) during the collapse of Poly-I in crowded aqueous solutions. (b) Contributions to the total polymer-solvent energy change during polymer collapse, including changes in intrapolymer energy ($\Delta E_{pp}^{E \rightarrow C}$), polymer-water interaction energy ($\Delta E_{pw}^{E \rightarrow C}$), polymer-crowder interaction energy ($\Delta E_{pc}^{E \rightarrow C}$), and polymer-counterion interaction energy (ΔE_{p-ci}^E). Reprinted under the terms of the Creative Commons Attribution License from ref [105]. 146
- 5.8 (a) Radial distribution functions of the polymer-crowder interaction for (a) CR- and (b) CR+ in the C- and E-states of Poly-I. (c) The average number of water and crowder molecules in the first solvation shell of Poly-I. The x-axis values correspond to the average solvent-accessible surface area (SASA) of Poly-I in various aqueous solutions (in nm²). The snapshots depict the spatial density distribution of crowders in the first solvation shell of the C- and E-states of Poly-I. (d, e) Probability distributions of tetrahedral order ($P(q_{tet})$) of water molecules around the termini and the side chains of the central region of Poly-I in the E-state within the first solvation shell in CR- and CR+ solutions, respectively. Solid lines represent solutions with crowders, while dotted lines represent solutions without crowders. Reprinted under the terms of the Creative Commons Attribution License from ref [105]. 147

- 5.9 (a) Changes in the polymer-solvent energy ($\Delta E_{pv}^{E \rightarrow C}$) and entropy ($\Delta S_{pv}^{E \rightarrow C}$) during the collapse of Poly-II in crowded aqueous solutions. (b) Contributions to the total polymer-solvent energy change during polymer collapse, including changes in intrapolymer energy ($\Delta E_{pp}^{E \rightarrow C}$), polymer-water interaction energy ($\Delta E_{pw}^{E \rightarrow C}$), polymer-crowder interaction energy ($\Delta E_{pc}^{EC \rightarrow C}$), and polymer-counterion interaction energy ($\Delta E_{p-ci}^{E \rightarrow C}$). Reprinted under the terms of the Creative Commons Attribution License from ref [105]. 148
- 5.10 (a) Radial distribution functions of the polymer-crowder interaction for (a) CR- and (b) CR+ in the C- and E-states of Poly-II. (c) The average number of water and crowder molecules in the first solvation shell of Poly-II. The x-axis values correspond to the average solvent-accessible surface area (SASA) of Poly-II in various aqueous solutions (in nm²). The snapshots depict the spatial density distribution of crowders in the first solvation shell of the C- and E-states of Poly-II. (d, e) Probability distributions of tetrahedral order ($P(q_{tet})$) of water molecules around the termini and the side chains of the central region of Poly-II in the E-state within the first solvation shell in CR- and CR+ solutions, respectively. Solid lines represent solutions with crowders, while dotted lines represent solutions without crowders. Reprinted under the terms of the Creative Commons Attribution License from ref [105]. 150
- 5.11 The schematic representation of the branched polymer in a CR- solution illustrates the surfactant-like behavior of crowders. 152
- 6.1 The β -hairpin from 2GB1 protein. (a) The 3D structure of the C-terminal fragment of a peptide containing β -sheet (yellow). (b) The schematic depiction of the structure revealing the pattern of hydrogen (orange) bonds and interaction (blue) between hydrophobic core residues that stabilise the β -hairpin structure (c) two different types of charged crowders, positively charged (CR+) and negatively charged (CR-). 156
- 6.2 The initial configuration of the system includes a β -sheet in three different environments: (a) a solution of only water molecules, (b) a solution containing CR+, (c) a solution containing CR-. And the blue spheres represent the ions. 158

-
- 6.3 2D probability distribution, with R_g^{core} on the x-axis and $\text{RMSD}^{\text{core}}$ on the y-axis, for the folded (F) state without crowders in (a), the unfolded (U) state without crowders in (d), the unfolded state in the presence of CR- in (e), and the unfolded state in the presence of CR+ in (f). 163
- 6.4 2D distributions of Ramachandran angles for the hydrophobic core residues of the peptide in (a-c) F ensembles and (d-f) U ensembles in pure water and crowded solutions. 164
- 6.5 The interaction energy of individual amino acid residues of the β -hairpin peptide with water molecules ($U_{\text{res-water}}$) and with crowder molecules ($U_{\text{res-crowder}}$) for (a), (b) the F ensemble and (c), (d) the U ensemble. The highlighted residues on the x -axis indicate the hydrophobic core residues. 165
- 6.6 The image illustrates the preferential binding coefficient (Γ) of the crowders on the surface of the peptide. The left panel represents Γ in the folded state for CR- crowders, while the right panel demonstrates it in the folded state for CR+ crowders. 167
- 6.7 The image illustrates the preferential binding coefficient (Γ) of the crowders on the surface of the peptide. The left panel represents Γ in the unfolded state for CR- crowders, while the right panel demonstrates it in the unfolded state for CR+ crowders. 168
- 7.1 The image illustrates the future outlook of the work presented in this thesis. (A) This image depicts a cartoon representation of liquid-liquid phase separation (LLPS) in immune-related diseases. Reprinted with permission from ref [294] Copyright 2022 Springer Nature. (B) This image demonstrates the dense phase stability of crowders in IDPs systems. Reprinted under the terms of the Creative Commons Attribution License from ref [295]. (C) This cartoon representation highlights the opportunity to improve the force field of a mixed, crowded environment. Reprinted under the terms of the Creative Commons Attribution License from ref [80] (D) This image illustrates a system of heterogeneous or mixed crowded environments where size and excluded volume effects become significant. . . 180

ABBREVIATIONS

MD	Molecular Dynamics
RDF	Radial distribution function
IDP	Intrinsically disordered protein
PES	Potential energy surface
LLPS	Liquid-Liquid phase separation
REMD	Replica Exchange Molecular Dynamics
SA	Simulated Annealing
AMD	Accelerated Molecular Dynamics
SMD	Steered Molecular Dynamics
KBI	Kirkwood-Buff Integral
R-KBI	Running-Kirkwood-Buff Integral
K-KBI	Krüger-corrected Kirkwood-Buff Integral
G-KBI	Ganguly-corrected Kirkwood-Buff Integral
B-KBI	Both-corrected Kirkwood-Buff Integral
EG	Ethylene glycol
PEG	Poly-ethylene glycol
DP	Degree of polymerization
Poly-I	Linear polymer
Poly-II	Branched polymer
SASA	Solvent-accessible surface area
PMF	Potential of mean force
RMSD	Root Mean Square Deviation

SYMBOLS NOTATION

$W_s(r)$	Depletion potential
V_{ov}	Overlap volume
$\Gamma_{23}(r_p)$	Preferential binding coefficient of the co-solute (3) on solute (2) molecules
k_B	Boltzmann constant
R	Gas constant
T	Temperature
Λ_{db}	de Broglie wavelength
V^b	Biased potential
V^u	Unbiased potential
G	Gibbs free energy
$G_{ij}(r)$	Kirkwood-Buff integral
g_{ij}	Radial distribution function
$w(r)$	Potential of mean force
$\Delta G^{u \rightarrow b}$	Change in free energy from unbound to bound state
$\Delta E_{dv}^{u \rightarrow b}$	Change in enthalpy from unbound to bound state
$\Delta S_{dv}^{u \rightarrow b}$	Change in entropy from unbound to bound state
a_{33}	Derivative of $\ln a_3$ (activity of crowders) w.r.t. crowders concentration (c_3)
μ_{23}^M	Chemical potential derivative of component 2 (PIC dyes) as a function of component 3 (EG) concentration
Γ_{23}^A	Preferential binding coefficient of EG to dye molecules in the aggregated (A) state
Γ_{23}^D	Preferential binding coefficient of EG to dye molecules in the dispersed (D) state
μ^*	Excess chemical potential
ϕ	Interaction energy between solute (polymer)-solvent (comprising crowder and water)
$\Delta G^{E \rightarrow C}$	The change in free energy of polymer collapse

$\Delta S_{pv}^{E \rightarrow C}$	Total entropy change during the transition from extended (E) to collapse (C) state
$CR+$	Positively charged crowders
$CR-$	Negatively charged crowders
R_g	Radius of gyration
$\omega_i^b(R_g)$	Harmonic bias potential
k_b	Force constant
$R_{g,i}^{\text{ref}}$	Desired equilibrium value of the reaction coordinate
N_c	Number of the crowders
R_g^{core}	Radius of gyration of the core residues
q_{tet}	Tetrahedral order metric